Atom-diatom scattering dynamics of spinning molecules

C. J. Eyles, J. Floß, I. Sh. Averbukh, and M. Leibscher

Citation: The Journal of Chemical Physics **142**, 024311 (2015); doi: 10.1063/1.4905251
View online: http://dx.doi.org/10.1063/1.4905251
View Table of Contents: http://scitation.aip.org/content/aip/journal/jcp/142/2?ver=pdfcov
Published by the AIP Publishing

Atom-diatom scattering dynamics of spinning molecules

C. J. Eyles,[1] J. Floß,[2] I. Sh. Averbukh,[2] and M. Leibscher[3,a)]
[1]*Institut für Chemie und Biochemie, Freie Universität Berlin, 14195 Berlin, Germany*
[2]*Department of Chemical Physics, Weizmann Institute of Science, Rehovot 76100, Israel*
[3]*Institut für Theoretische Physik, Leibniz Universität Hannover, 30167 Hannover, Germany*

(Received 26 February 2014; accepted 18 December 2014; published online 12 January 2015)

We present full quantum mechanical scattering calculations using spinning molecules as target states for nuclear spin selective atom-diatom scattering of reactive D+H_2 and F+H_2 collisions. Molecules can be forced to rotate uni-directionally by chiral trains of short, non-resonant laser pulses, with different nuclear spin isomers rotating in opposite directions. The calculations we present are based on rotational wavepackets that can be created in this manner. As our simulations show, target molecules with opposite sense of rotation are predominantly scattered in opposite directions, opening routes for spatially and quantum state selective scattering of close chemical species. Moreover, two-dimensional state resolved differential cross sections reveal detailed information about the scattering mechanisms, which can be explained to a large degree by a classical vector model for scattering with spinning molecules. © *2015 AIP Publishing LLC.* [http://dx.doi.org/10.1063/1.4905251]

I. INTRODUCTION

Since the encounter of two reacting species depends on their relative orientation, the outcome of a chemical reaction can be manipulated by controlling the rotational state of the reacting molecules. A prototypical reaction is the reactive collision between an atom and a diatom. The study and control of reactive collision mechanisms as a function of reactant and product molecule polarisation has been the subject of extensive study in recent years.[1–3] A powerful method to control the rotational dynamics of molecules is to excite rotational wavepackets with moderately strong, non-resonant laser pulses (see, e.g., Ref. 4). A single short pulse creates a rotational wavepacket that shows transient alignment after the interaction. With properly designed sequences of laser pulses, one can achieve a high degree of control over the rotational wavepacket, e.g., enhance the degree of alignment,[5] excite uni-directional rotation,[6–8] or selectively excite high rotational states in a mixture of different species.[9,10] The scattering of molecules by inhomogeneous electric fields[11] or at surfaces[12] can be influenced by pre-exciting rotational wavepackets. Rotating molecules are scattered at different angles than rotationally cold molecules.

Homonuclear diatomic molecules occur in the form of different nuclear spin isomers which can be distinguished by their rotational spectrum. *Para*-H_2, for example, consists of rotational states with even values of the rotational quantum number j, while *ortho*-H_2 has only odd rotational states. As a consequence, rotational wavepackets of different nuclear spin isomers show characteristic differences in their dynamics which can be employed to selectively excite rotations for a specific isomer.[10,13] It was suggested that the combination of nuclear spin selective control of rotational dynamics with surface scattering might lead to a spatial separation of nuclear spin isomers or other close chemical species, for example, molecular isotopes.[14] In a similar spirit, atom-diatom collisions in the gas phase have been considered for the reactions D + H_2 and F + H_2 with *para* (*p*-) and *ortho* (*o*-) H_2.[15] As has been demonstrated in Ref. 10, a sequence of two properly delayed laser pulses can enhance the rotational excitation of one nuclear spin isomer while suppressing it for the second isomer. The different distributions of rotational states affect the scattering process, and strongly nuclear spin selective reaction rates can thus be achieved.[15] Moreover, the differential cross-sections reveal different reaction mechanisms for rotationally excited and rotationally cold molecules. In order to use rotational wavepackets as target states for the control of atom-diatom collisions, one has to take into account the different time scales involved. Rotational dynamics are much faster than the scattering process. The transient features of the rotational dynamics will have no influence on the outcome of the reaction. However, the average alignment considerably affects the outcome of atom-diatom reactions.[15]

Another interesting aspect is how the sense of rotation of the reactant molecules influences the reaction dynamics.[2] This requires the preparation of the molecules in rotational states with a superposition of magnetic sub-levels.[16] Molecules can be prepared in rotational states with non-zero average angular momentum, i.e., with the preferred sense of rotation by sequences of linear polarised laser pulses with different polarisations. The use of a chiral train of short laser pulses has been demonstrated to be particularly efficient in exciting such uni-directionally rotating molecules.[17–19] In this study, we propose to use such chiral pulse trains to excite rotational wavepackets with non-zero average momentum as target states for scattering experiments and investigate how the sense of rotation determines the spatial distribution of the scattered molecules. Spinning molecules are of particular interest as target states for atom-diatom scattering since they possess a non-vanishing average angular momentum which leads to scattering cross-sections that depend, in contrast to conventional

a)Author to whom correspondence should be addressed.

scattering experiments, on the azimuthal as well as on the polar scattering angle.

The parameters of a chiral pulse train can be chosen such that the rotational motion can be induced in a nuclear spin selective fashion. For example, a single isomer can be selectively excited, or clockwise rotation is induced in one isomer and counter-clockwise rotation in the other. In the following, we present calculations for the scattering of $D+H_2$ and $F+H_2$ with uni-directionally rotating wavepackets of p-H_2 and o-H_2 which have been excited using a chiral pulse train chosen such that the two nuclear spin isomers rotate in opposite directions. We demonstrate that, although the nuclear spin is not used in the scattering calculations, the product molecules resulting from reactions with p-H_2 and o-H_2 are scattered in different directions. Moreover, we find that the two-dimensional differential cross sections offer valuable mechanistic insights into the scattering mechanism of uni-directionally rotating molecules, in particular with respect to the spatial distribution of the scattered molecules.

II. THEORY

A. Calculation of quantum mechanical observables from the transition matrix

We consider the scattering of diatomic molecules with atoms, as shown in Fig. 1. Prior to the scattering event, the molecules are prepared by a chiral train of laser pulses[19] such that they are spinning with a preferential sense of rotation. In a classical picture, the motion of the uni-directionally rotating molecules is confined to a plane, here to the ZY-plane, with the angular momentum oriented perpendicular to the plane in the $+X$ or $-X$ direction, depending on the sense of rotation (note that the space-fixed X-axis defined in Fig. 1 does not depend on the sense of rotation of the molecules). The duration of the laser pulses is short compared to the rotational period, so that rotational wavepackets

$$|\Psi(t)\rangle = \sum_{jm} b_{jm}(t)\,|jm\rangle \tag{1}$$

are excited. Here, $j = 0, 1, 2, \ldots$ and $-j \le m \le j$ are the rotational quantum numbers of a linear rotor. The expansion coefficients after the end of the interaction are specified by a constant initial value and a time dependent phase

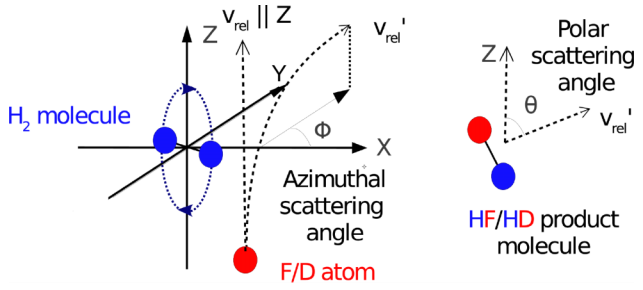

FIG. 1. Depiction of the space fixed collision frame (X, Y, Z) employed in this work. The Z-axis is defined by the direction of the incoming relative velocity v_{rel}. The polar (θ) and azimuthal (ϕ) scattering angles describe the direction of the product molecule for reactive collisions.

$$b_{jm}(t) = c_{jm}\exp\left(-i\frac{Bj(j+1)\,t}{\hbar}\right), \tag{2}$$

where B is the rotational constant of the diatom.

The solution of the close-coupled equations describing the quantum mechanical scattering of a diatomic molecule with a structureless particle is a solved problem and is now a relatively routine process.[20–23] Solution of these equations yields a set of transition matrix ($\hat{T}$-matrix) elements specifying the individual channel-to-channel probability amplitudes. In reactive systems, such calculations are complicated by the different possible molecular arrangements in the entrance and exit channels; the "abc" quantum scattering code[23] employed in this work solves this ambiguity by simultaneously considering all three chemical arrangements using hyper-spherical coordinates, in which the problem becomes isomorphic to the simpler case of non-reactive inelastic scattering. The $\hat{T}$-matrix elements are calculated in the body fixed helicity frame, where the helicity quantum number specifies the projection of **j** onto the relative linear momentum of the atom-diatom pair.

If the target state is a rotational wavepacket, the $\hat{T}$-matrix elements can be written as a coherent superposition of the conventional eigenstate-to-eigenstate $\hat{T}$-matrix elements, such that

$$\langle j'k'|\hat{T}^{JM}|\Psi(t)\rangle = \sum_{jk} b_{jk}(t)\,\langle j'k'|\hat{T}^{JM}|jk\rangle. \tag{3}$$

Here, jk and $j'k'$ denote the rotational and helicity projection quantum numbers of the initial and final states, respectively, and JM denotes the total angular momentum quantum number and (space fixed) projection quantum number. Note that for the initial state (in which the incoming linear momentum lies along the $+Z$ axis), the helicity frame quantisation axis and the space fixed quantisation axis coincide exactly, and we have the convenient result $c_{jk} = \exp(ik\phi)c_{jm=k}$, and $|jk\rangle = \exp(-ik\phi)|jm\rangle$, where ϕ is the azimuthal angle between the space fixed and helicity frame X-axes, which is equivalent to the space fixed azimuthal scattering angle.

In a typical scattering experiment, the exact timing of the collision relative to the rotational phase of the diatom cannot be controlled. The duration of a typical molecular beam pulse has a lower limit on the order of tens of μs, many orders of magnitude higher than the rotational period, and so even if the individual collision events themselves can be considered to be instantaneous, any experimentally observed results will be averaged over the time dependence of the rotational wavepacket. In this case, the averaging over the time dependence is equivalent to an averaging out of the coherences existing between all states with different values of j. In terms of the density matrix describing the wavepacket, the elements that are off-diagonal in j all average out to zero over time, while the diagonal elements (again in j) remain unchanged.[24] However, the coherences between different m sub-levels within a particular rotational state are time independent and hence survive the average over t. This is a crucial point as it implies that the axial asymmetry of a wavepacket with oriented angular momentum distribution is present as a time averaged phenomenon. What remains upon taking a time average can thus no longer be described as a pure state.

One of the most elementary observables associated with a scattering event is the integral collision cross-section, which is related to the probability with which a collision affects a particular transition. The state-to-state resolved collision cross-sections can be written in terms of the helicity frame $\hat{T}$-matrix elements as

$$\sigma_{j'k'jk} = \frac{\pi}{k_{\text{vec}}^2} \sum_J (2J+1) \left|\langle j'k'|T^J|jk\rangle\right|^2, \tag{4}$$

where k_{vec} is the wave-vector associated with the collision. The transition matrix elements $\langle j'k'|T^J|jk\rangle$ give the probability amplitude for the transition from the initial state $|jk\rangle$ to the final state $|j'k'\rangle$ for the Jth partial wave. The time-averaged integral cross-section, resulting from scattering with an initial rotational wavepacket then reads

$$\sigma_{j'k'} = \frac{\pi}{k_{\text{vec}}^2} \sum_J (2J+1) \sum_j \left|\sum_k c_{jk} \langle j'k'|T^J|jk\rangle\right|^2. \tag{5}$$

These collision cross-sections effectively provide a snapshot of the two vector $\mathbf{j}-\mathbf{k}$ correlation for the particular angular momentum polarisation corresponding to our choice of rotational wavepacket. While they give us information on the likely outcome of the collision process, they are somewhat lacking in detailed dynamical or mechanistic information concerning the conformation of the colliding particles and their detailed relative motions. Such information is instead best obtained from other (higher order) vector properties, in particular from the differential cross-sections; quantifying the scattering angle dependence of the cross-section gives a highly detailed insight into the collision dynamics.[25,26] By transforming from the spherical wave basis to a plane wave basis, the state-to-state resolved differential cross-section can be written in terms of the helicity frame $\hat{T}$-matrix elements as

$$\frac{\mathrm{d}\sigma}{\mathrm{d}\omega}_{j'k'jk}(\theta) = \frac{4\pi^2}{k_{\text{vec}}^2} \left|\sum_J \frac{2J+1}{4\pi} d^J_{k'k}(\theta) \langle j'k'|\hat{T}^J|jk\rangle\right|^2, \tag{6}$$

where $d^J_{k'k}(\theta)$ is a reduced Wigner rotation matrix element.[33] In this work the collision geometry is defined such that the H_2 molecule lies at the origin of the space fixed frame, with the atomic partner's relative velocity directed along the $+Z$ axis. The scattering angle θ is then given by the polar angle of the outgoing scattered HF or HD diatom, as shown in Fig. 1. As such, forward scattering ($\theta = 0$) corresponds to the HF or HD product molecule travelling in the same direction as the initial F or D atom. Note that the conventional eigenstate-to-eigenstate differential cross-sections do not depend on the azimuthal scattering angle. This is because the initial and final states are both cylindrically symmetric in the collision frame, and so there is nothing to distinguish one azimuthal angle from any other. The coherences between different m sub-levels within a particular rotational state, which are created by the chiral pulse train, lead to a breaking of the axial symmetry. As a result, the differential cross-section depends on the polar angle θ as well as on the azimuthal angle ϕ

$$\frac{\mathrm{d}\sigma}{\mathrm{d}\omega}(\theta,\phi) = \frac{4\pi^2}{k_{\text{vec}}^2} \sum_j \left|\sum_k c_{jk} \sum_J \frac{2J+1}{4\pi} D^{J*}_{k'k}(\phi,\theta,-\phi) \langle j'k'|\hat{T}^J|jk\rangle\right|^2. \tag{7}$$

Note that the formulae for the time averaged integral and differential cross-sections yield analytically identical results to those that would be obtained by calculating the fully time dependent cross-sections for each individual time point in the evolution of the fully coherent wavepacket and subsequently averaging over the time interval of one rotational revival period $t_{rev} = \hbar\pi/B$.

In recent studies, the theoretical groundwork for describing the stereodynamics of atom-diatom reactions distinguishes between the preparation of the reactant polarisation (referred to as the extrinsic polarisation) and the conversion of this initial state into the product polarisation (which is controlled by the so called intrinsic polarisation of the reaction).[1–3] Such quantities are typically represented in terms of the so called polarisation dependent differential cross-sections,[27–32] which allow a complete and concise mathematical description of the various vector correlations associated with the collision process, or in terms of the more intuitive stereodynamics portraits.[1,2] In this study, we show instead two-dimensional differential cross-sections which offer an alternative visualisation of the reaction dynamics of the rotational wavepackets. The advantage of the two-dimensional differential cross sections is that they highlight the spatial distribution of product molecules arising from the reaction of a uni-directionally rotating wavepacket.

B. Calculation details

The quantum reactive scattering package "abc"[23] was used to generate the requisite $\hat{T}$-matrix elements for the reactive scattering calculations performed in this work. The Liu-Siegbahn-Truhlar-Horowitz potential energy surface (PES)[34–36] was used for the calculations on $D + H_2$, and the Stark-Werner PES[37] was employed for the $F + H_2$ system. Since each individual scattering calculation is run at a fixed *total* energy, each different initial rotational quantum state is associated with a different *collision* energy. For this reason, it was necessary to run a separate scattering calculation for each initial rotational state, adjusting the total energy so as to obtain a constant collision energy of 1.00 eV for $D + H_2$ and 0.05 eV for $F + H_2$. In order to converge the scattering calculations, it is necessary to specify the size of the basis sets used and the manner in which the integration of the close-coupled equations is carried out. For the $D + H_2$ reaction at a collision energy of 1.00 eV, a rotational basis up to $j = 25$ was employed, including states up to a maximum energy of 3.2 eV, and propagation was carried out up to a maximum hyper-radius of 12 bohrs, divided into 200 sectors. Partial waves up to $J = 50$ and helicity projection quantum numbers up to $k_{\text{max}} = 5$ were included to ensure convergence of the $\hat{T}$-matrix elements.[40] For the $F + H_2$ reaction at a collision energy of 0.05 eV, a rotational basis up to $j = 25$ was employed, including states up to a maximum energy of

3.2 eV, and propagation was carried out up to a maximum hyper-radius of 12 bohrs, using 150 sectors. Inclusion of partial waves up to $J = 30$ and helicity projection quantum numbers up to $k_{max} = 4$ were sufficient to converge the reactive cross-sections (see also Refs. 15, 41, and 42).

III. EXCITATION OF SPINNING MOLECULES WITH A CHIRAL PULSE TRAIN

In order to investigate the effect of the sense of rotation on atom-diatom reactions, the reactant molecules have to be prepared in rotational states with non-zero angular momentum. A chiral train of non-resonant laser pulses, as depicted in Fig. 2, allows the excitation of uni-directionally rotating wavepackets.[17–19] Moreover, the parameters of the pulse train can be chosen such that different nuclear spin isomers rotate in opposite directions. The pulses are linearly polarised, but with a constant angular shift δ of the polarisation axis from pulse to pulse (see Fig. 2). The time-delay τ between subsequent pulses is constant. By adjusting the pulse-to-pulse polarisation angular shift δ and the time-delay τ, one can control the populations of the angular momentum states as well as the sense of the molecular rotation (see below). The strength of an individual pulse can be described by the reduced interaction strength $P = \Delta\alpha/(4\hbar)\int dt\mathcal{E}^2(t)$, where $\Delta\alpha$ is the polarisability anisotropy of the molecule and $\mathcal{E}$(t) is the envelope of the electric field. The reduced interaction strength corresponds to the typical amount of angular momentum (in units of $\hbar$) transferred to the molecule by the pulse. We consider a pulse train like the one used in the experiment described in Ref. 17, where the strength of the nth pulse is given as

$$P_n = P_{tot}J_n^2(A). \tag{8}$$

Here, $P_{tot} = \sum P_n$ is the total interaction strength, J_n is the Bessel function of first kind, and A is a parameter. Such a train contains approximately $2A$ non-zero pulses. In our simulations, we use $P_{tot} = 8$ and $A = 4$. The pulse duration is 25 fs (full width at half maximum of the intensity envelope). We consider a mixture of p-H_2 (even j) and o-H_2 (odd j) and assume that the molecules are initially in their respective rotational ground states $j = 0$ (p-H_2) and $j = 1$ (o-H_2). This corresponds to a rotational temperature of $T \approx 100$ K, at which the fraction of p-H_2 and o-H_2 molecules residing in the rotational ground state would be 97.5% and 99.995%, respectively.

FIG. 2. A train of linearly polarised laser pulses interact with linear molecules. The polarisation axis is rotated by an angle δ between each pulse, and the time-delay between the pulses is constant.

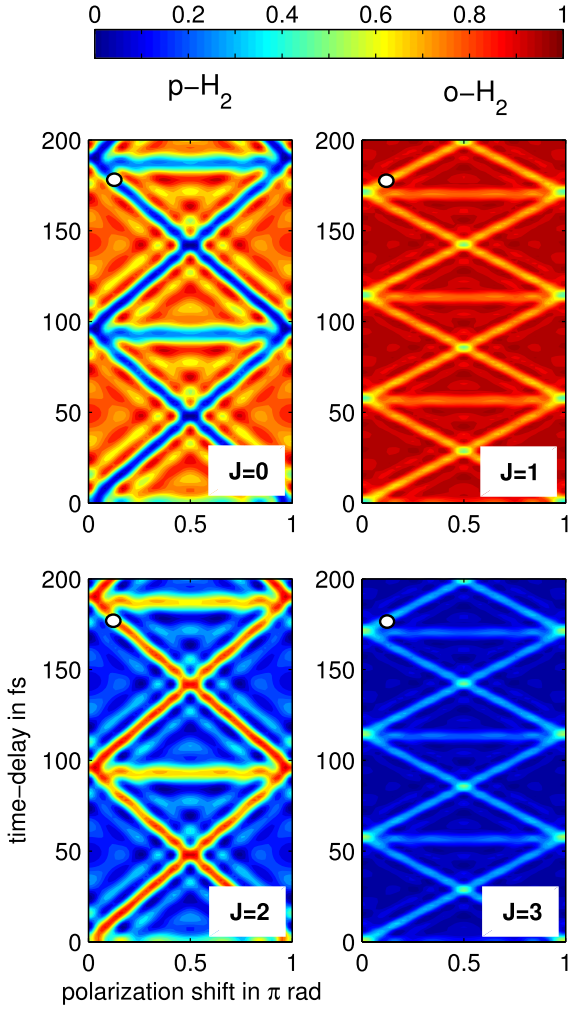

FIG. 3. Population $Q(j)$ of the rotational levels $j = 0$ and $j = 2$ for p-H_2, and for $j = 1$ and $j = 3$ for o-H_2 at $T = 100$ K after interacting with a pulse train with $A = 4$ (see text). The total reduced pulse strength is $P_{tot} = 8$, and the FWHM of each pulse is 25 fs. The white dots indicate the values $\tau = 177.3$ fs and $\delta = 0.1175\pi$ rad.

The population $Q(j)$ of the rotational levels j for *para*- and *ortho*-hydrogen after interaction with the considered pulse train is shown in Fig. 3 as a function of the delay time τ between the individual pulses and the pulse-to-pulse polarisation shift δ. The lines of strong excitation are described by

$$\tau = t_{exc}(j)\left(m + \Delta m\frac{\delta}{2\pi}\right), \tag{9}$$

with $\Delta m = 0, \pm 2$ and $t_{exc}(j) = t_{rev}/(2j-1)$. Lines with $\Delta m = 2$ (up-slope in Fig. 3) correspond to a wavepacket rotating counter-clockwise, $\Delta m = -2$ (down-slope in Fig. 3) to clockwise, and $\Delta m = 0$ (no slope) to a wavepacket with no preferred rotational sense. Using Eq. (9), one can select parameters for which the pulse train excites clockwise rotation in p-H_2 and counter-clockwise rotation in o-H_2. For example, using the parameters $\tau = 177.3$ fs and $\delta = 0.1175\pi$ rad, indicated by the white dots in Fig. 3, a clockwise rotating wavepacket of p-H_2 is excited, consisting mainly of the $|0,0\rangle$ and $|2,-2\rangle$ states, and a counter-clockwise rotating wavepacket of o-H_2 consisting

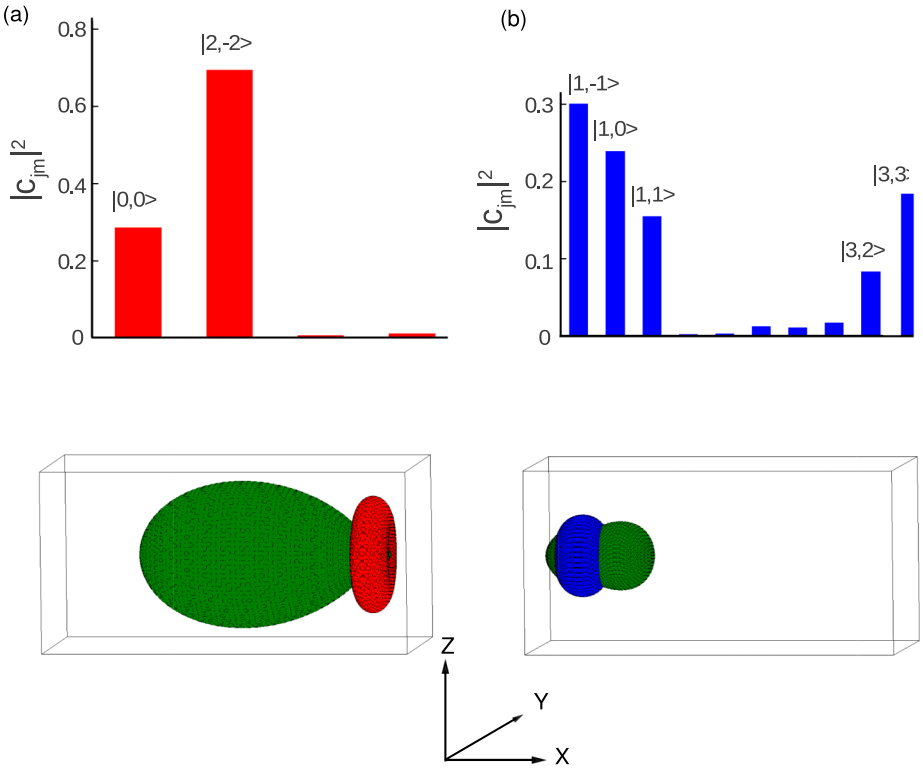

FIG. 4. Populations $|c_{jm}|^2$ (in the laser frame) of the rotational eigenstates in the p-H_2 (panel (a), red) and o-H_2 (panel (b), blue) wavepackets after excitation with a chiral pulse train with the parameters $P_{tot} = 8$, $A = 4$, $\tau = 177.3$ fs, and $\delta = 0.1175\pi$ rad (see text). The pulse duration is 25 fs (FWHM), and the initial rotational temperature $T \approx 100$ K. The lower panels show the bond axis and angular momentum distributions of the p-H_2 and o-H_2 wavepackets (calculated as described in main text). The corners of the boxes are given by $-0.2 \le Y, Z \le 0.2$, $-0.7 \le X \le 0.1$ (a), and $-0.1 \le X \le 0.7$ (b), with X, Y, and Z denoting the collision frame. Bond axis distribution plots are shown in red and blue, and rotational angular momentum distribution plots are shown in green.

mainly of the $|1,-1\rangle$, $|1,0\rangle$, and $|1,1\rangle$, and the $|3,1\rangle$, $|3,2\rangle$, and $|3,3\rangle$ states. The coefficients of these rotational wavepackets, as well as the bond axis and angular momentum distributions,[39] are depicted in Fig. 4. In the case of o-H_2, these distributions were calculated assuming an initial equal population of the $|1,0\rangle$ and $|1,\pm1\rangle$ eigenstates, each of which forms a separate rotational wavepacket after exposure to the laser pulse train. The expansion coefficients of each wavepacket were used to calculate the bond axis and rotational angular momentum distributions, and an ensemble average was then taken over the three wavepackets.

It should be noted that although there is, in particular for the p-H_2 wavepacket, a strong net angular momentum pointing along the X axis, the wavepacket is not *exclusively* unidirectionally rotating and although the bond axis polarisation is quite tightly confined within the ZY plane, is not exclusively limited to within its confines, as must necessarily be the case for a quantum mechanical rotor. The average angular momentum of the p-H_2 wavepacket is more strongly oriented than the angular momentum of the corresponding o-H_2 wavepacket. This is because the p-H_2 wavepacket is formed exclusively from the $|0,0\rangle$ eigenstate, undergoing highly selective excitation to the $|2,-2\rangle$ eigenstate. In contrast, the o-H_2 wavepacket is formed from a statistical mixture of the $|1,-1\rangle$, $|1,0\rangle$, and $|1,1\rangle$ eigenstates, each of which are selectively excited to the $|3,1\rangle$, $|3,2\rangle$, and $|3,3\rangle$ eigenstates, respectively. This range of spatially directed populated eigenstates reduces the specificity of the rotational polarisation of the o-H_2 wavepacket compared to the simpler p-H_2 case.

In the laser frame (see Fig. 2), the wavepacket, when averaged over time, is axially symmetric, and so would not yield any azimuthal dependence in its scattering dynamics if the colliding atom was to approach along the laser frame z axis. For this reason, the collision frame is chosen so that the molecular bond axis distribution lies preferentially in the ZY plane, with the net rotational angular momentum pointing along the $\pm X$ axis (see Fig. 1). The incoming D/F atom then approaches vertically upwards along the $+Z$ direction, colliding with the axially asymmetric wavepacket of H_2 molecules. Because of the difference between the two frames, the eigenstate populations given in Fig. 4 are no longer valid in the collision frame and must be rotated into this frame to perform the relevant scattering calculations via the expression[33]

$$c_{jm}^{\text{coll}} = \sum_{m'} d_{mm'}^{j}(\Theta_{\text{coll}})\, c_{jm'}^{\text{laser}}, \tag{10}$$

where Θ_{coll} defines the orientation of the collision frame with respect to the laser frame. In our case, where the Z axis of the collision frame coincides with the x axis of the laser frame, we have $\Theta_{\text{coll}} = \pi/2$. Table I shows the expansion coefficients for the coherent superposition of eigenstates obtained by rotating the most strongly populated p-H_2 eigenstates from the laser frame into the collision frame. In the laser frame, the magnetic eigenstates initially exist in a statistical mixture, with

TABLE I. Expansion coefficients of the clockwise rotating p-H_2 wavepacket in the laser and collision frame.

Laser frame	Collision frame
$c_{00} = 0.5334$	$c_{00} = 0.5334$
$c_{2-2} = 0.8459$	$c_{2-2} = 0.2115$
	$c_{2-1} = -0.4230$
	$c_{20} = 0.5180$
	$c_{21} = -0.4230$
	$c_{22} = 0.2115$

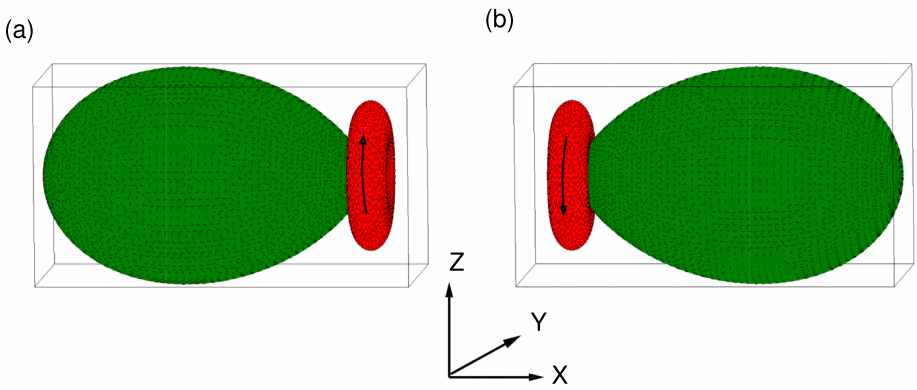

FIG. 5. Bond axis distribution (red) and angular momentum distribution (green) of the rotational state $|2, -2\rangle$ (a) and $|2, 2\rangle$ (b), rotated by 90°. The corners of the boxes are given by $-0.2 \leq Y, Z \leq 0.2$, $-0.7 \leq X \leq 0.1$ (a), and $-0.1 \leq X \leq 0.7$ (b), with X, Y, Z denoting the collision frame. The arrows indicate the sense of rotation. The D-atoms approach vertically upwards along the $+Z$ direction.

no coherences between the various magnetic sub-levels, and hence the bond axis and rotational angular momentum distributions are cylindrically symmetric in this frame. After rotation into the collision frame, each individual eigenstate gives rise to a coherent superposition of magnetic sub-levels, yielding a cylindrically asymmetric bond axis and rotational angular momentum distribution.

IV. ATOM-DIATOM SCATTERING DYNAMICS

In the following, we present a case study of the reactive scattering dynamics for uni-directionally rotating molecules and investigate how the spatial distribution of the product molecules depends on the sense of rotation of the reagent molecules. We mainly consider the $D + H_2$ reaction at a collision energy of 1.00 eV as model system, as well as the $F + H_2$ reaction at a collision energy of 0.05 eV. For all reactive differential cross-sections presented here, the scattering angles θ and ϕ are defined as (1) the polar angle between the outgoing relative velocity of the product HF or HD molecule and the incoming relative velocity of the F or D atom, and (2) as the azimuthal angle of the scattered HF or HD product molecule, respectively, as shown in Fig. 1. In this case, $\theta = 0$ corresponds to forward scattering of the product molecule, and $\phi = 0$ corresponds to the HD or HF molecule being scattered in the $+X$ direction of the XY plane of the collision frame.

A. Scattering dynamics for molecules with oriented angular momentum

To start with, we consider the $D + H_2$ reaction with H_2 initially in the rotational state $|j,\pm j\rangle$ rotated by 90° for $j = 1, 2, 3$. The bond axis and angular momentum distributions[39] are shown in Fig. 5 for $|2,\pm 2\rangle$, rotated by 90°. Since the average angular momenta are oriented in the +X or −X direction, the bond axis distribution has a disc-like shape centred in the ZY-plane. The D-atoms approach vertically upwards along the +Z direction, i.e., the cylindrical symmetry is broken, and the differential cross sections depend on both the polar angle θ and the azimuthal angle ϕ. Therefore, we analyse the scattering

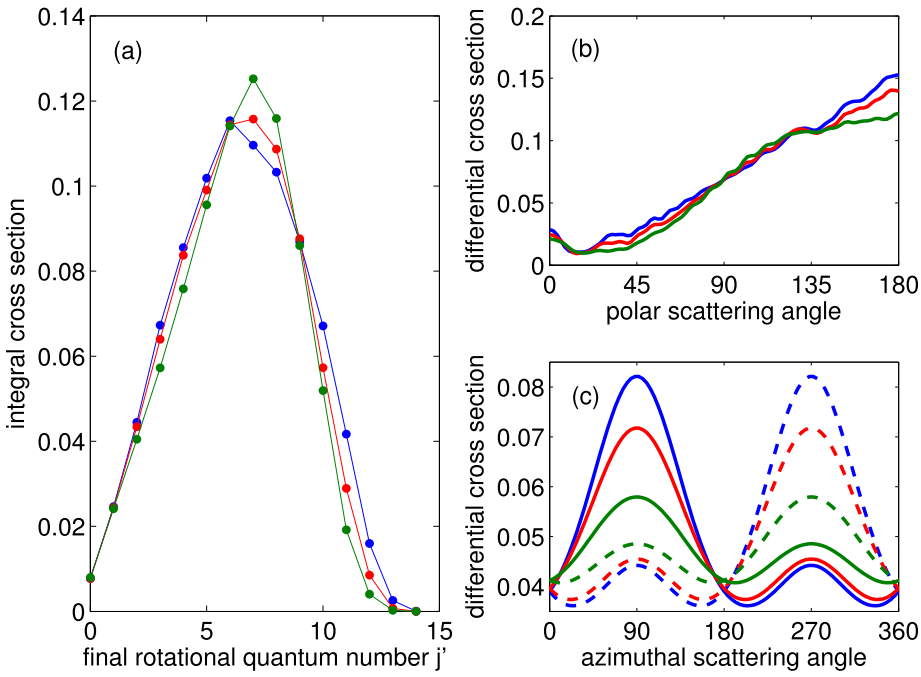

FIG. 6. Integral cross section (a) and total reactive differential cross section along the polar angle θ, integrated over ϕ (b) and along the azimuthal angle ϕ, integrated over θ (c) for reactive ($v' = 0$) $D + H_2$ scattering at a collision energy of 1.00 eV. The initial states are $|j, \pm j\rangle$ rotated by 90°, with $j = 1$ (green), $j = 2$ (red), and $j = 3$ (blue). The azimuthal cross section for the states $|j, j\rangle$ and $|j, -j\rangle$ are depicted in solid and dashed lines, respectively.

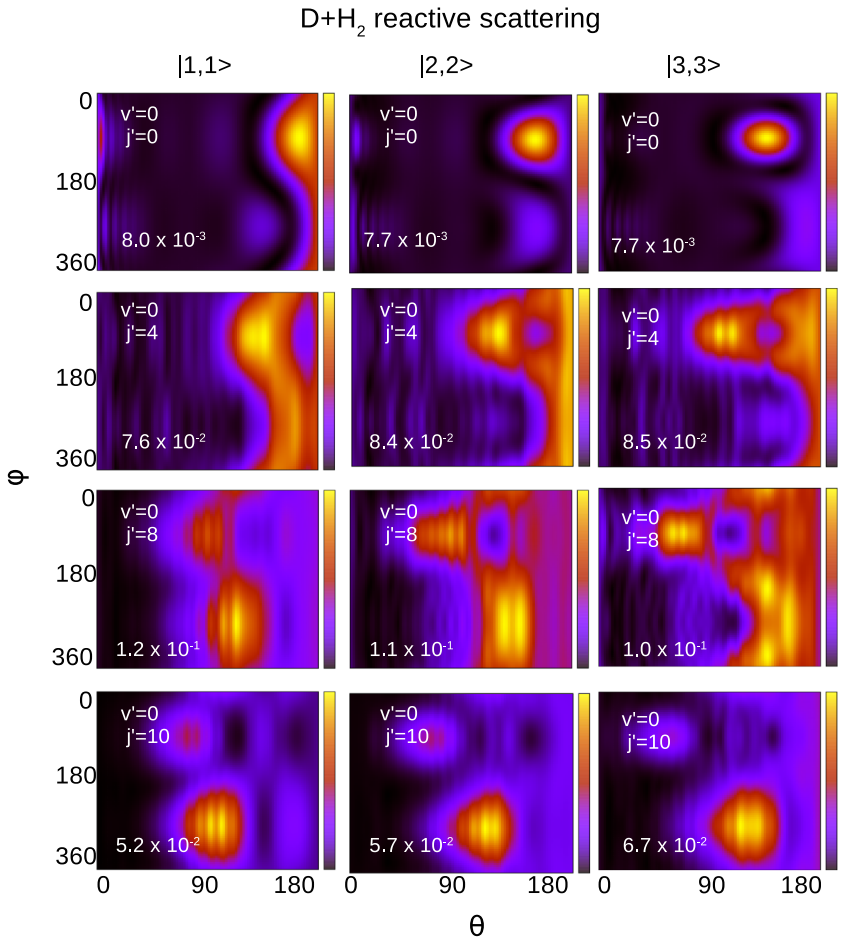

FIG. 7. State to state resolved two dimensional differential cross-sections for molecules in the initial state $|j, j\rangle$ rotated by 90° in the D + H_2 reaction at a collision energy of 1.00 eV for $j = 1, 2, 3$. The horizontal axes show the conventional polar scattering angle θ, and the vertical axes depict the azimuthal scattering angle ϕ. The colour scales are normalised separately for each panel, running from zero to the maximum value of the two-dimensional differential cross-section, and so reflect only the directional distribution of the scattered products. The corresponding absolute magnitude of the collision cross-section in units of $Å^2$ is given in each panel.

dynamics by considering the differential cross sections along the polar angle (integrated over ϕ) and along the azimuthal angle ϕ (integrated over θ) as well as the two-dimensional differential cross sections. The integral and differential cross sections for the initial states with $j = 1, 2, 3$ are shown in Fig. 6. The main contribution to the reactive integral cross section comes from the $v' = 0$ product channel, i.e., the product HD molecules are rotationally excited but remain in their vibra-

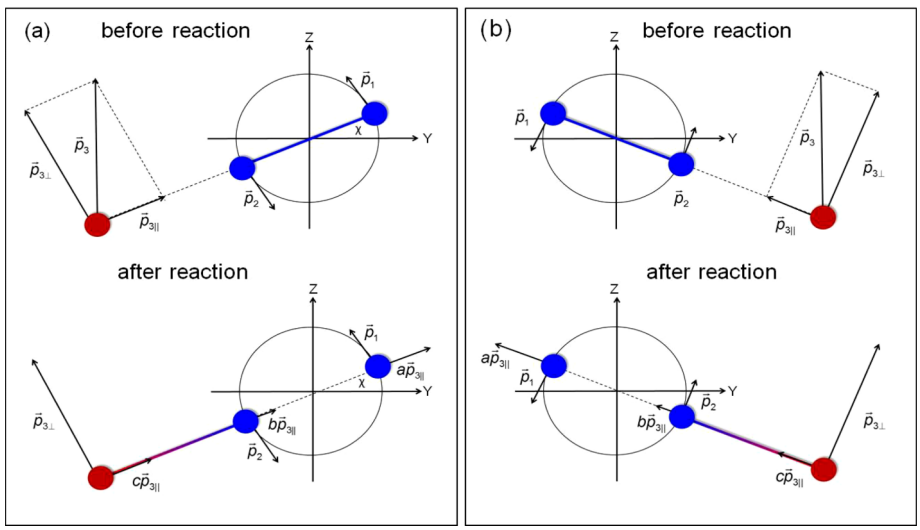

FIG. 8. Reactive collision of a spinning diatomic molecule with an atom approaching on the left side (a) and on the right side (b) of the spinning atom. The figure shows the linear momenta of the three atoms before and after the reaction.

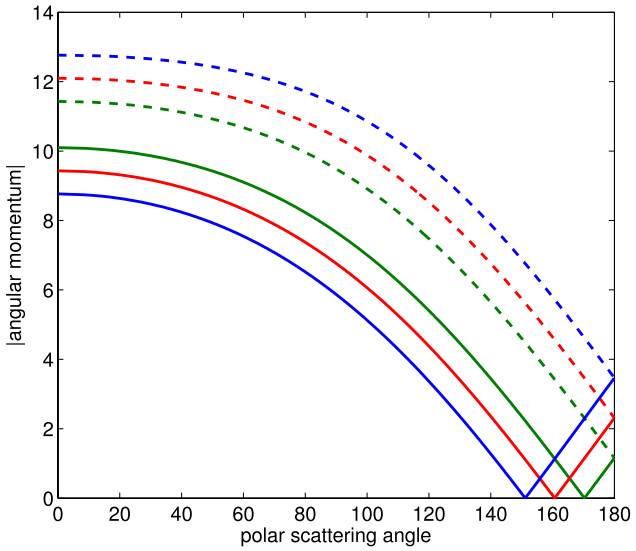

FIG. 9. Absolute value of the final angular momentum (in units of $\hbar$) as a function of the polar scattering angle for reactive collisions D + H_2. The solid (dashed) curves correspond to an azimuthal scattering angle of $\phi = 90°$ ($\phi = 270°$). Green, red, and blue curves correspond to a initial angular momentum corresponding to $j = 1$, 2, and 3, respectively.

tional ground state (see, e.g., Refs. 15, 38, and 40). Neither the integral cross-sections nor the polar differential cross-sections depend on the sense of rotation of the wavepacket. In fact, the form of the integral and polar differential cross-sections is very similar to that observed for a spherically symmetric distribution of H_2 molecules as considered in a conventional scattering experiment.[15,38,40] This is an apparent contradiction to Ref. 2, where it is stated that the excitation of high or low product rotational states depend on the angular momentum polarization. We will discuss this below. However, the azimuthal differential cross section shown in panel (c) of Fig. 6 is determined by the sense of rotation of the reagent molecules. Note that the azimuthal differential cross section for counter-clockwise rotating initial states follows directly from the one for clockwise rotating states. For our application to clockwise and counter-clockwise rotating wavepackets of *o*-H_2 and *p*-H_2, it is nevertheless useful to show both cases. It can be seen that the azimuthal differential cross section has peaks at $\phi = 90°$ and $\phi = 270°$. This is a result of the approximate confinement of the molecules to the ZY-plane. Since the dominant reaction mechanism for the D+H_2 reaction is a direct reaction,[1,2] it occurs mainly when the three atoms are co-planar, corresponding to $\phi = 90°$ and $\phi = 270°$. With increasing j, the confinement of the bond axis distribution to the ZY-plane is stronger, and thus, the scattering in the $\phi = 90°$ and $\phi = 270°$ directions is more pronounced. Moreover, the orientation of the angular momentum determines the azimuthal direction of the scattered molecules; if the angular momentum points toward $+X$ (counter clockwise rotation), the product molecules are scattered predominantly to the right ($\phi = 90°$); if the angular momentum points toward $-X$ (clockwise rotation), the product molecules are scattered predominantly to the left ($\phi = 270°$). But a minor peak is also observed in the opposite direction.

The final state resolved two-dimensional differential cross section is shown in Fig. 7 for counter-clockwise rotating states. (The two-dimensional differential cross sections for clockwise rotating states are not shown here. They are identical to Fig. 7 except that the azimuthal scattering angles are reversed.) It reveals that the azimuthal scattering direction depends on the product rotational state. Product molecules with low j' are scattered mainly in $\phi = 90°$ direction while states with high j' are scattered in $\phi = 270°$ direction. In other words, for a fixed azimuthal angle, e.g., $\phi = 90°$, counter-clockwise rotating states produce product molecules with low j' while clockwise rotating states lead to product states with high j'. For $\phi = 270°$, the behaviour is reversed. We employ a classical vector model as outlined in Ref. 2 to explain the underlying reaction mech-

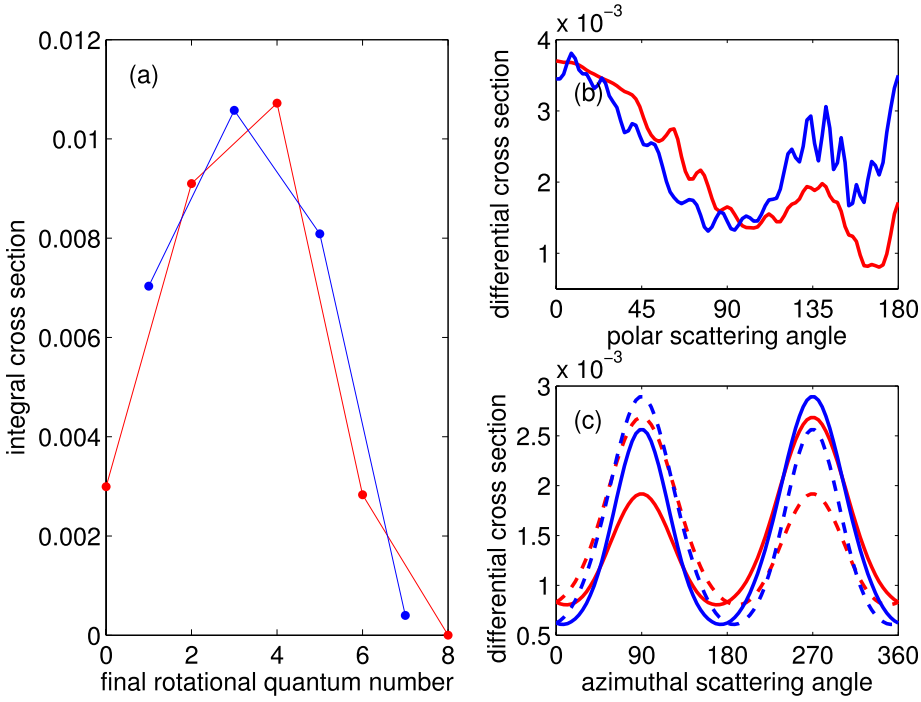

FIG. 10. Integral cross section (a) and total non-reactive differential cross section along the polar angle θ, integrated over ϕ (b) and along the azimuthal angle ϕ, integrated over θ (c) for vibrationally inelastic ($v' = 1$) D+H_2 scattering at a collision energy of 1.00 eV. The initial states are $|j, \pm j\rangle$ rotated by 90°, with $j = 2$ (red) and $j = 3$ (blue). The azimuthal cross section for the states $|j, j\rangle$ and $|j, -j\rangle$ is depicted in solid and dashed lines, respectively.

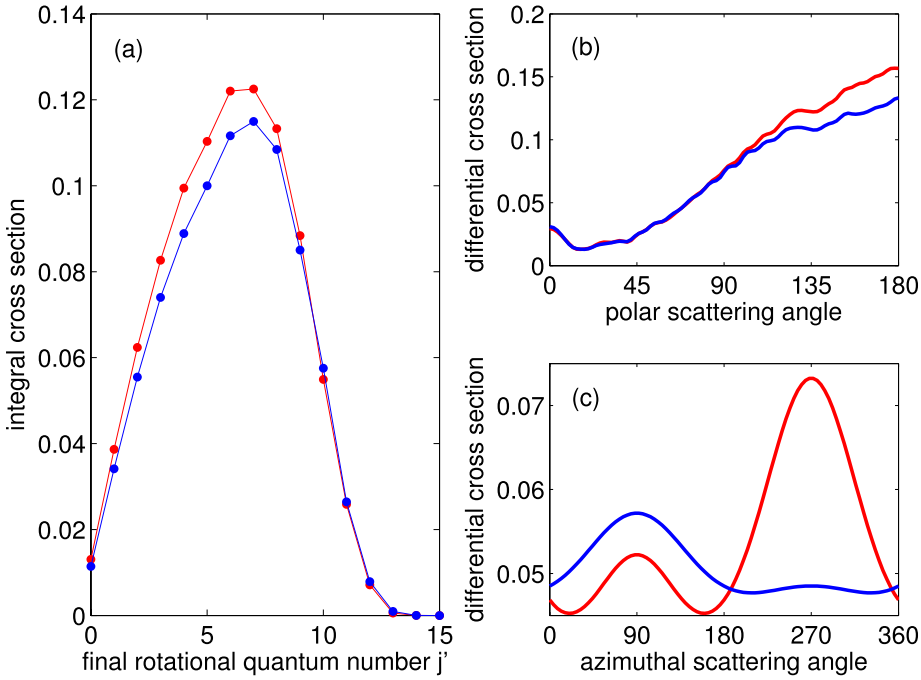

FIG. 11. Integral cross section (a) and total reactive differential cross section along the polar angle θ, integrated over ϕ (b) and along the azimuthal angle ϕ, integrated over θ (c) for reactive ($v' = 0$) D + H_2 scattering at a collision energy of 1.00 eV for p-H_2 (red) and o-H_2 excited by a chiral train of laser pulses such that p-H_2 rotates predominantly clockwise (angular momentum pointing in the −X direction) and o-H_2 anti-clockwise (angular momentum pointing in the +X direction).

anism. It is assumed that the collision can be described by a sample of classical rigid rotors rotating in a plane and colliding with structureless particles, as shown in Fig. 8. In this model, the disc-like shape of the bond axis distribution is idealised, and the motion of the atoms is restricted to the ZY-plane. The model implies a linear transition state since bent transition states allow reactive collisions with atoms outside the plane in which the molecules rotate. Moreover, it is assumed that the reactions is instantaneous compared with rotational timescales, implying a direct collision mechanism.[1,2] Qualitative conclusions can already be drawn from the sketch shown in Fig. 8. The figure shows counter-clockwise rotating molecules with angular momentum in +X direction. The D-atoms can approach from the left side, as in panel (a) or from the right side as shown in panel (b). Assume that the rotational momenta ($\vec{p}_1$ and $\vec{p}_2$) of the molecule are much larger than the translational momentum ($\vec{p}_3$). In this case, the sense of rotation dictates the azimuthal scattering direction: for positive initial angular momentum, the product molecules are scattered entirely to the right ($\phi = 90°$). Moreover, the direction of the rotation with respect to the target molecule is reversed, in much the same way as two interlinking gears must necessarily rotate in opposite directions when transferring their rotational motion to one another. If the translational momentum is larger than the initial rotational momentum, the azimuthal scattering direction is determined by the approaching atom. For a D-atom approaching from the left side, the product H-atom is scattered to the right and the product molecule is scattered to the left ($\phi = 270°$), and vice versa if the D-atom approaches from the right. As it is already argued in Ref. 2, the product molecules are in a high rotational state if the component $\vec{p}_{3\perp}$ of the translational momentum (see Fig. 8) is anti-parallel to the rotational momentum. For target molecules with positive angular momentum, this is the case if the atom approaches from the left [Fig. 8(a)]. Thus, the product molecules with high j' are scattered to the left ($\phi = 270°$). If the atom approaches from the right [Fig. 8(b)], the (initially positive) angular momentum is parallel to the $\vec{p}_{3\perp}$ of the translational momentum which leads to product states with low j', which are scattered to the right ($\phi = 90°$). For the initial states with $j = 1$, 2, and 3, the translational momentum is larger than the rotational momentum, and thus the second mechanism applies, which is in accordance with the two-dimensional differential cross sections shown in Fig. 7. For the same reason, clockwise rotating molecules are scattered in the opposite directions.

Figure 8 also explains the apparent contradiction of our results that the polar cross section is independent of the angular momentum (see Fig. 6(b)) with the contrary statement in Ref. 2. Here, we simulate a possible experiment where the molecules are prepared, prior to the scattering process, in a state with oriented angular momentum. An incoming atom approaches the molecule either from the left or from the right side, as shown in Figs. 8(a) and 8(b), respectively. For atoms approaching from the left, the argument given in Ref. 2 holds, namely, that high or low final rotational states are favoured if the reactant angular momentum is oriented in $+X$ or $-X$ direction, respectively. However, the atom can also approach from the right. In this case, molecules with angular momentum oriented in the $+X$ ($-X$) direction lead to low (high) final angular momenta. As a net result, for the scattering angles defined as in Fig. 1, the polar differential cross section, integrated over all values of ϕ, does not depend on the angular momentum distribution but the azimuthal differential cross section does.

The classical vector model also provides a more quantitative description of the scattering process. As we detail in the Appendix, it predicts, for given initial angular momentum, the final angular momentum as a function of the scattering angles. In Fig. 9, we show the absolute value of the final angular momentum $L_X^{(f)}$ in units of $\hbar$ as a function of the scattering

angle according to the classical model for molecules with initial angular momentum corresponding to $j = 1$, 2, and 3. For $L_X^{(f)} = 0$, the classical model predicts backward scattering in the $\phi = 90°$ direction, with slightly decreasing polar scattering angle for increasing initial rotational number. Moreover, for all initial states, it is predicted that the polar scattering angle for this collision pathway decreases for higher final rotational states, leading to more sideways scattering. For $L_X^{(f)} = 4\hbar$ (corresponding to $j' = 4$), the classical model also shows a second scattering pathway in the $\phi = 270°$ direction, which starts in the backward direction. The polar scattering angle for this pathway also decreases as higher final rotational states are accessed. All those effects can be observed in the two-dimensional state resolved cross-section of the quantum mechanical calculations, shown in Fig. 7. These results indicate that the model of classical rigid rotors in a plane provides a valid description of the dominant collision mechanism for the reactive scattering of D atoms with spinning H_2 molecules.

There are at least two effects which cannot be explained by the classical vector model. Due to the restriction to planar scattering, the classical model presented here cannot explain the large, backward-scattering peaks in the differential cross section which are more or less independent of ϕ. This can be accounted for by the fact that for scattering angles close to 180°, the product molecules are effectively distributed on a very narrow cone and changing the azimuthal direction does not have a big effect. This is compounded by the fact that, in reality, the reaction can progress through a transition state which is not perfectly linear. These two points account for the largely ϕ-independent distribution of products for near backward scattering. Moreover, for initial $j = 1$ and $j = 2$, scattering in the $\phi = 90°$ direction to $j' \geq 10$ is classically forbidden, as can be seen from Fig. 9. Nevertheless, the quantum mechanical differential cross sections have a weak peak in this direction.

Next, we investigate the spatial distribution of the scattered molecules in the case of non-reactive vibrationally inelas-

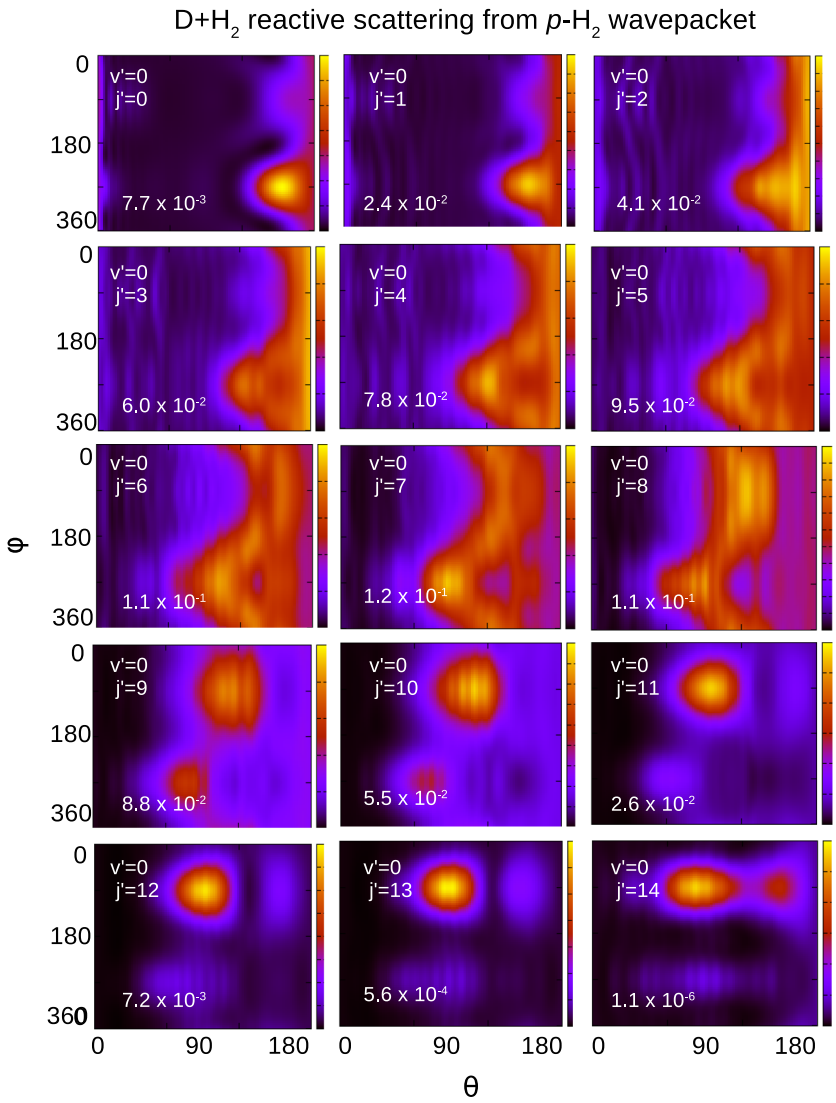

FIG. 12. Final quantum state resolved two dimensional differential cross-sections of the p-H_2 wavepacket in the D + H_2 reaction at a collision energy of 1.00 eV. The horizontal axes show the polar scattering angle θ, and the vertical axes depict the azimuthal scattering angle ϕ. Each panel corresponding to a particular final quantum state has been normalised separately, so the colour coding reflects only the directional distribution of scattered product, and not the absolute magnitude of the scattering cross-section. The absolute value of the scattering cross-section in units of Å^2 is written in each panel.

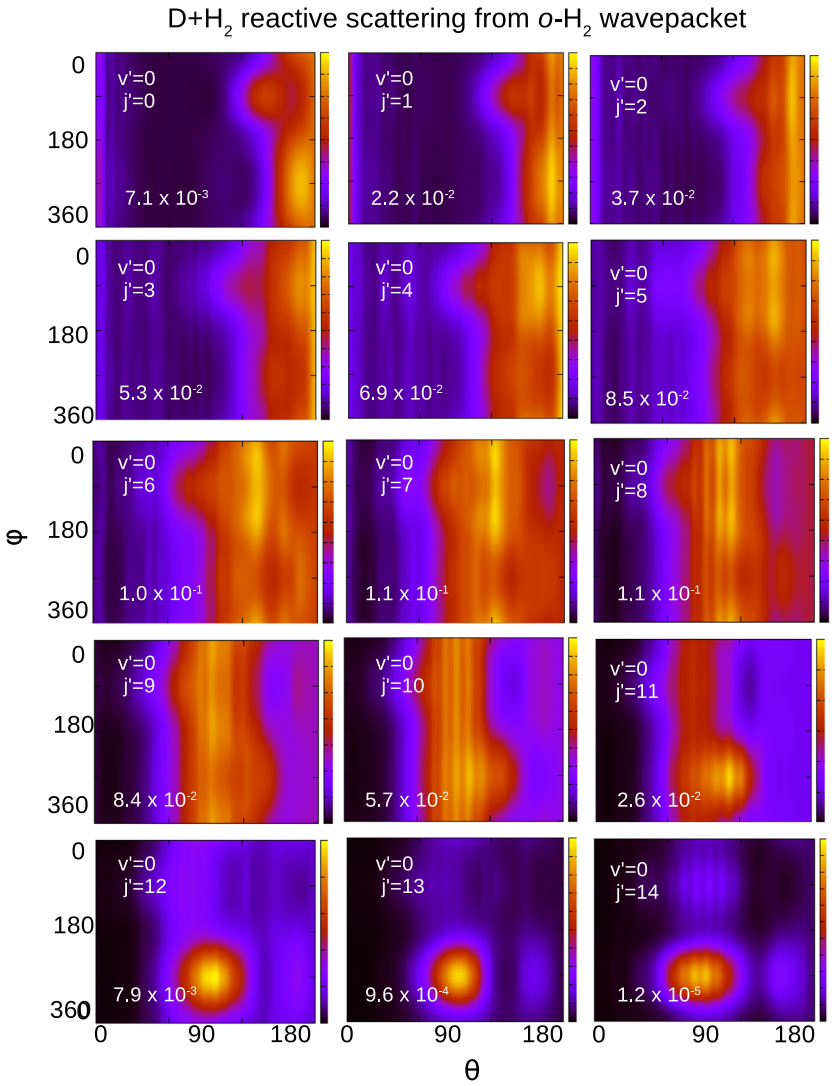

FIG. 13. Final quantum state resolved two dimensional differential cross-sections of the o-H_2 wavepacket in the D + H_2 reaction at a collision energy of 1.00 eV. The horizontal axes show the polar scattering angle θ, and the vertical axes depict the azimuthal scattering angle ϕ. Each panel corresponding to a particular final quantum state has been normalised separately, so the colour coding reflects only the directional distribution of scattered product, and not the absolute magnitude of the scattering cross-section. The absolute value of the scattering cross-section in units of Å^2 is written in each panel.

tic D+H_2 scattering. The integral and differential cross sections for the initial states $|j,\pm j\rangle$ rotated by 90° are shown in Fig. 10 for j = 1, 2 ,3. Here, the angles θ and ϕ denote the outgoing direction of the scattered D atom. The main contribution to the inelastic scattering cross section is the v' = 1 channel. Note that the total reactive cross-section is around 20 times larger than the total vibrationally inelastic cross-section. For non-reactive collisions, the parity of the rotational states is conserved, i.e., only even (odd) states are excited from states with even j and odd j, respectively. The cylindrical asymmetry of the rotational wavepackets leads to a ϕ-dependent differential cross section for inelastic scattering as well. An asymmetry of the ϕ-dependence can be observed: for counter-clockwise rotating molecules (angular momentum pointing in +X-direction), the D-atoms are more likely to be scattered in $\phi = 90°$ direction than in the $\phi = 270°$ direction and vice versa. However, the asymmetry is far less pronounced than for reactive scattering, especially for $j = 3$. Since reactive scattering is much more sensitive to the sense of rotation of the target molecules than non-reactive scattering, we concentrate on reactive scattering.

B. Application to mixture of *p*-H_2 and *o*-H_2 excited by a chiral train of laser pulses

As an application, we consider a mixture of p-H_2 and o-H_2 at $T \approx 100$ K. As explained in Sec. III, a chiral pulse train can excite rotational wavepackets such that p-H_2 rotates clockwise and o-H_2 rotates anti-clockwise. The bond axis and angular momentum distributions of the p-H_2 wavepacket are very similar to that of the rotated $|2,-2\rangle$ eigenstate. The o-H_2 wavepacket consists of states with positive and negative angular momentum. While contributions with positive angular momentum prevail, the confinement of the bond-axis distribution to a plane is less pronounced than for the p-H_2 wavepacket. Figure 11 displays the integral and the polar and azimuthal differential cross-sections for the reactive scattering of the D + H_2 reaction, where the initial state of the H_2 molecules

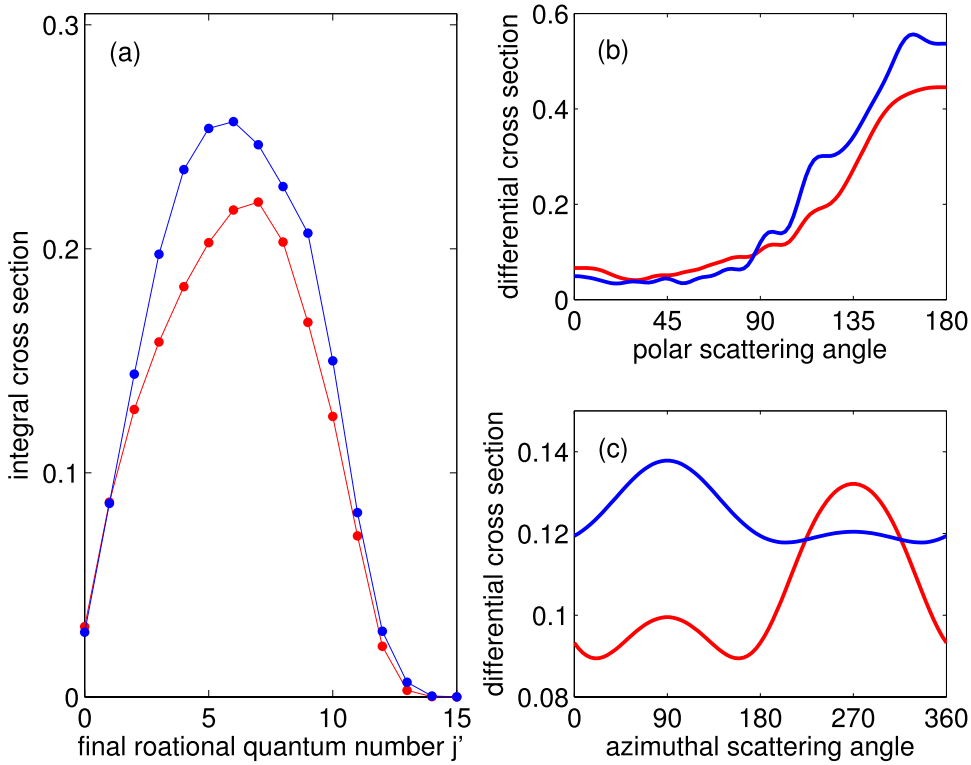

FIG. 14. Reactive $v' = 2$ collisions of the F + H_2 system at a collision energy of 0.05 eV. The figure shows the integral cross section (a) and total reactive differential cross section along the polar angle θ, integrated over ϕ (b) and along the azimuthal angle ϕ, integrated over θ (c) for p-H_2 (red) and o-H_2 excited by a chiral train of laser pulses such that p-H_2 rotates predominantly clockwise (angular momentum pointing in the −X direction) and o-H_2 anti-clockwise (angular momentum pointing in the +X direction).

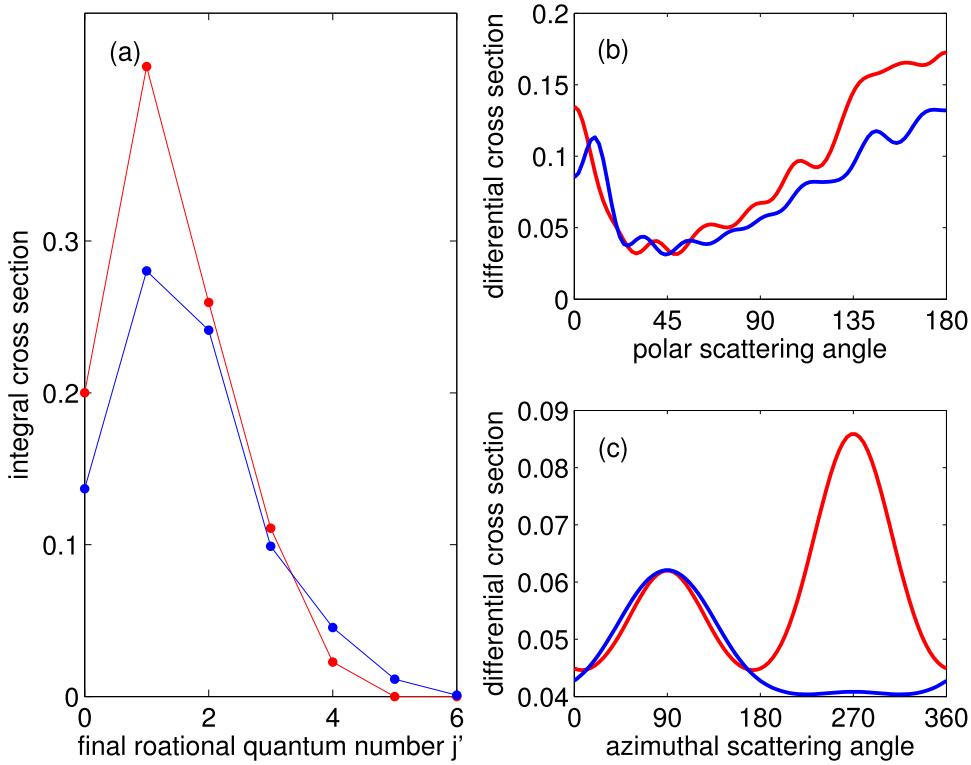

FIG. 15. Reactive $v' = 3$ collisions of the F + H_2 system at a collision energy of 0.05 eV. The figure shows the integral cross section (a) and total reactive differential cross section along the polar angle θ, integrated over ϕ (b) and along the azimuthal angle ϕ, integrated over θ (c) for p-H_2 (red) and o-H_2 excited by a chiral train of laser pulses such that p-H_2 rotates predominantly clockwise (angular momentum pointing in the −X direction) and o-H_2 anti-clockwise (angular momentum pointing in the +X direction).

is given by the uni-directionally rotating wavepackets defined in Fig. 4. The red curves present the clockwise rotating *p*-H_2, while the blue curves present *o*-H_2 which rotates counter-clockwise. The small differences between *p*-H_2 and *o*-H_2 in the integral cross-sections [Fig. 11(a)] and polar differential cross-sections [Fig. 11(b)] are a result of the different j states populated in the *p*-H_2 and *o*-H_2 wavepackets. The azimuthal differential cross-sections [Fig. 11(c)] differ substantially for the *p*-H_2 and *o*-H_2 wavepackets, reflecting the opposite sense of rotation of the two wavepackets, as discussed above. Product molecules are observed to be preferentially scattered in the plane of the H_2 molecular rotation ($\phi = 90°$ and $\phi = 270°$), as expected. The azimuthal differential cross-section is more sharply peaked for the *p*-H_2 wavepacket than for the *o*-H_2 analogue. This is a reflection of the greater degree of polarisation that was obtained for the *p*-H_2 wavepacket compared to the *o*-H_2 wavepacket in the excitation stage using the chiral train of short laser pulses. However, we also see that the directional preference for reactive scattering is reversed on going from *p*-H_2 to *o*-H_2. This implies that careful selection of the precise nature of the chiral pulse train employed to excite the rotational wavepacket can be used to cause the products of the D + H_2 reaction to preferentially scatter into a desired range of azimuthal angles, in a nuclear spin dependent fashion. Figure 12 displays the two-dimensional final state resolved differential cross section for the clockwise rotating *p*-H_2 wavepacket. Comparison with Fig. 7 clearly indicates that the scattering is dictated by the rotated $|2,-2\rangle$ eigenstate. The corresponding information for the counter-clockwise rotating *o*-H_2 wavepacket is shown in Fig. 13. In this case, the azimuthal angular distributions are somewhat blurred due to the reduced sharpness of the rotational angular momentum polarisation of the *o*-H_2 wavepacket. Even so, the preferred azimuthal scattering angle for the population of a given quantum state can be seen to be reversed compared to the clockwise rotating *p*-H_2 wavepacket, and the same trend in the reversal of the preferred azimuthal scattering angle from low j' to high j' is clearly visible once more.

Preferential scattering directions for scattering with spinning molecules are not restricted to D + H_2 collisions. Figs. 14 and 15 show a similar set of integral and differential cross-sections for the dominant $v' = 2$ and $v' = 3$ product channels of the F + H_2 reaction, respectively. In this case, the *p*-H_2 wavepacket slightly favours the $v' = 3$ product channel over the lower energy $v' = 2$ vibrational manifold.[15,43,44] This is a direct consequence of a Feschbach resonance connecting the $v = 0$, $j = 0$ initial quantum state, and the $v' = 3$, $j' = 1$ final quantum state, and is quite specific to the F + H_2 reaction, and to the particular collision energy of 0.05 eV. Apart from this small detail, the integral and the conventional differential cross-sections for the clockwise rotating *p*-H_2 and the anti-clockwise rotating *o*-H_2 wavepackets are quite similar to one another, while the azimuthal directional dependencies are once again opposite to one another, implying a certain degree of spatial separation of product molecules resulting from clockwise or anti-clockwise rotating target states. The assumptions applied in the classical model (see the Appendix) are in good agreement with the D + H_2 → HD + H reaction. In particular, the reaction has a rather tightly confined linear transition state, and it is isoenergetic. For reactive F + H_2 scattering, these conditions are not fulfilled. The reaction is highly exothermic and has a bent transition state, which lifts the restriction of the scattering process to the plane of the spinning molecules. Therefore, while the general trend of the azimuthal differential cross sections is the same as for the D + H_2 → HD + H reaction, a direct comparison with the classical vector model is not applicable here.

V. CONCLUSIONS

We have investigated the scattering of an atom with a uni-directionally rotating diatomic molecule for the D + H_2 and F + H_2 reactive collisions. With a chiral train of laser pulses,[17–19] uni-directional rotation can be excited in linear molecules, inducing a rich range of collision dynamics. In particular, the spatial distribution of the scattered product molecules exhibits an azimuthal angular dependence as well as the usual polar angular dependence when the axial symmetry of the scattering geometry is broken. As a prototypical reaction, the isotopic variants of the H + H_2 reaction have been studied extensively, including the effects of reactant polarisation.[1–3] In this context, the role of the *sense of rotation* of the reactant molecules on the reaction dynamics has been discussed in Ref. 2. Here, we have investigated how the spatial distribution of the product molecules depends on the sense of rotation of the reagent molecules prepared in states with oriented angular momentum. The spatial distribution is highlighted by the two-dimensional differential cross sections shown here.

In particular for the D + H_2 reaction considered here, the azimuthal distribution of the scattered molecules is largely confined to the plane of rotation of the H_2 molecule and is also dictated to a large degree by the sense of rotation of the spinning molecules. This angular distribution is also highly sensitive to the final quantum state of the scattered product molecule. For the dominant direct reaction mechanism, the rotational states and spatial distribution of the scattered molecules can be explained by a simple classical vector model. Such a vector model has been outlined in Ref. 2 in order to qualitatively explain the role of the sense of rotation of the reactant molecules in determining the rotational state of the product molecule. Here, we extend this model and show that it also allows a quantitative description of the final state resolved scattering angles. Due to the nature of the reactive F + H_2 collision, in particular its exothermic behaviour and the bent transition state, the planar vector model cannot explain the details of this reaction. However, the main features which lead to preferential scattering in a direction sensitive to the initial sense of rotation are still present.

The simulations of the scattering dynamics show that target molecules which rotate in opposite directions are also predominantly scattered in opposite directions. This effect is much more pronounced for reactive scattering than for non-reactive scattering. Moreover, it can be increased by increasing the rotational energy of the target molecules relative to the collision energy. The preferential scattering can be employed for selective scattering of close chemical species. Here, we have demonstrated that, by carefully tuning the parameters of the chiral pulse train, the two nuclear spin isomers of

hydrogen, p-H_2 and o-H_2, can be forced to rotate in opposite directions. As a result, product molecules arising from p-H_2 are scattered predominantly in the opposite direction to molecules resulting from o-H_2. An additional application would be selective scattering of molecular isotopes, which also will be scattered in different directions and thus separated spatially, if one of the isotopes is forced to rotate clockwise, while the other rotates counter-clockwise. With a properly tuned chiral pulse train, one can also force one molecular species, e.g., a particular nuclear spin isomer, to rotate uni-directionally while another species can be aligned along a space fixed axis. For the scattering geometry applied here, molecules aligned along the collision frame X-axis are expected to be scattered in $\phi = 0$ and $\phi = 180°$ direction, while the molecules spinning in the ZY plane are scattered in $\phi = 90°$ and $\phi = 270°$ direction. Such a scenario might lead to better separation of molecular species in cases where preferential scattering direction of clockwise and counter-clockwise rotating molecules is not very pronounced, for example, for the case of non-reactive collisions.

ACKNOWLEDGMENTS

We gratefully acknowledge the support from the DFG (Project No. LE 2138/2-1). C. J. Eyles is likewise grateful for the receipt of an Alexander von Humboldt research fellowship in support of this work.

APPENDIX: A CLASSICAL VECTOR MODEL FOR A + B_2 COLLISIONS WITH SPINNING MOLECULES

We present a classical vector model to provide a quantitative assessment of the mechanism proposed in previous work.[2] We consider collisions of an atom A with a homonuclear diatom B_2. The molecules, described as a sample of classical rigid rotors with constant angular velocity, rotate either clockwise or counter-clockwise in the ZY-plane, as depicted in Fig. 8. Before collision, the total kinetic energy of the atom-diatom system is

$$T^{(i)} = T^{(i)}_{rot} + T^{(i)}_{trans} = \frac{1}{2\mu}(\vec{p}_{int})^2 + \frac{1}{2\mu_{trans}}(\vec{p}_{trans})^2, \quad \text{(A1)}$$

with $\mu = m_B/2$ and $\mu_{trans} = 2m_A m_B/(m_A + 2m_B)$, where m_A and m_B are the atomic masses of atoms A and B. Moreover,

$$\vec{p}_{int} = \frac{1}{2}(\vec{p}_1 - \vec{p}_2) \quad \text{(A2)}$$

and

$$\vec{p}_{trans} = \frac{2m_B}{m_A + 2m_B}\vec{p}_3 - \frac{m_A}{m_A + 2m_B}(\vec{p}_1 + \vec{p}_2). \quad \text{(A3)}$$

The atom has a constant momentum in the Z-direction with magnitude p_3 and the molecule is considered as rigid, i.e., no vibration is excited before the collision, and the molecule has only rotational energy

$$T^{(i)}_{rot} = \frac{1}{2\mu r_e^2}\left(L^{(i)}_X\right)^2 = \frac{p_2^2}{m_B} \quad \text{(A4)}$$

with $\vec{p}_2 = -\vec{p}_1$ perpendicular to the bond axis. Here, r_e is the bond length of the molecule. The total initial energy is thus

$$T^{(i)} = \frac{p_2^2}{m_B} + \frac{p_3^2}{m_A + 2m_B}\frac{m_B}{m_A}. \quad \text{(A5)}$$

Energy and momentum conservation allows us to determine the final angular momentum and the scattering angle for a particular collision event.

For reactive encounters, we assume a linear transition state, so that the reaction takes place when the atom and diatom form a straight line and the distance between the D atom and one of the H atoms equals the bond length of the product molecule, $r_e^{(f)}$ (see Fig. 8). Moreover, it is assumed that the reaction is isoenergetic and instantaneous compared to rotational time scales. For the reaction $D + H_2 \rightarrow HD + H$, these condition are fulfilled. Due to the momentum transfer during the reaction, the final momenta of the three atoms can be written as

$$\vec{p}^{(f)}_1 = \vec{p}_1 + a\vec{p}_{3\parallel}, \quad \text{(A6)}$$

$$\vec{p}^{(f)}_2 = \vec{p}_2 + b\vec{p}_{3\parallel}, \quad \text{(A7)}$$

$$\vec{p}^{(f)}_3 = \vec{p}_{3\perp} + c\vec{p}_{3\parallel}, \quad \text{(A8)}$$

with $a + b + c = 1$ assuring momentum conservation. Here, $p_{3\perp} = p_3 \cos\chi$ and $p_{3\parallel} = p_3 \sin\chi$ are the components of $\vec{p}_3$ perpendicular and parallel to the bond axis, and $\vec{p}_1$, $\vec{p}_2$, and $\vec{p}_3$ denote the linear momenta of the three atoms before the reaction. The angle χ is defined as shown in Fig. 8. The final kinetic energy is then

$$T^{(f)} = T^{(f)}_{int} + T^{(f)}_{trans} = \frac{1}{2\mu^{(f)}}\left(\vec{p}^{(f)}_{int}\right)^2 + \frac{1}{2\mu^{(f)}_{trans}}\left(\vec{p}^{(f)}_{trans}\right)^2. \quad \text{(A9)}$$

The reduced mass of the product molecule AB is $\mu^{(f)} = \frac{m_A m_B}{m_A + m_B}$ and

$$\mu^{(f)}_{trans} = \frac{m_B(m_A + m_B)}{m_A + 2m_B}. \quad \text{(A10)}$$

The internal momentum of the DH molecule is

$$\vec{p}^{(f)}_{int} = \frac{m_A}{m_A + m_B}\vec{p}^{(f)}_2 - \frac{m_B}{m_A + m_B}\vec{p}^{(f)}_3 = \vec{p}^{(f)}_{rot} + \vec{p}^{(f)}_{vib}. \quad \text{(A11)}$$

The part of the internal momentum perpendicular to the bond axis gives rise to molecular rotation with

$$\vec{p}^{(f)}_{rot} = \frac{1}{m_A + m_B}(m_A\vec{p}_2 - m_B\vec{p}_{3\perp}), \quad \text{(A12)}$$

while the part which is parallel to the bond axis describes vibrational motion

$$\vec{p}^{(f)}_{vib} = \frac{1}{m_A + m_B}(bm_A - cm_B)\vec{p}_{3\parallel}. \quad \text{(A13)}$$

If no vibration is excited during the reaction, $\vec{p}^{(f)}_{vib} = 0$ and $c = bm_A/m_B$. If the product molecule is vibrationally excited, the vibrational energy determines the ratio between b and c. The final angular momentum is thus

$$L^{(f)}_X = r^{(f)}_e p^{(f)}_{rot}, \quad \text{(A14)}$$

where $p_{rot}^{(f)}$ is the magnitude of the final rotational momentum. The final translational momentum can be written as

$$\vec{p}_{trans}^{(f)} = \frac{m_A+m_B}{m_A+2m_B}\vec{p}_1^{(f)} - \frac{m_B}{m_A+2m_B}\left(\vec{p}_2^{(f)}+\vec{p}_3^{(f)}\right) \quad \text{(A15)}$$

$$= -\left(\vec{p}_2 + \frac{m_B}{m_A+2m_B}\vec{p}_{3\perp}\right) + \alpha\vec{p}_{3\parallel}. \quad \text{(A16)}$$

The parameter

$$\alpha = \frac{m_A+m_B}{m_A+2m_B} - (b+c) \quad \text{(A17)}$$

can be determined from energy conservation, i.e., $T^{(i)} = T^{(f)}$. If the product molecule is in the vibrational ground state,

$$\alpha = \frac{m_A+m_B}{m_A+2m_B}\sqrt{\frac{2m_B^2}{m_A(m_A+m_B)}}. \quad \text{(A18)}$$

The scattering angle is determined by the direction of the final translational momentum. The angle

$$\rho = \arctan\frac{|\vec{p}_2 + \frac{m_B}{m_A+2m_B}\vec{p}_{3\perp}|}{\alpha p_{3\parallel}} \quad \text{(A19)}$$

defines the direction of the translational momentum with respect to the molecular axis. We calculate the final angular momentum and the angle ρ as a function of the angle χ (see Fig. 8) at the moment of the reaction (which corresponds to the collision with atoms with different distances from the Y-axis, i.e., with different impact parameters). This allows us to determine the scattering angle for product molecules with particular final angular momentum. As can be seen in Fig. 8, momentum transfer between an atom and a spinning molecule can occur via two different pathways. Figure 8 depicts a counter-clockwise rotating molecule, with initial angular momentum pointing in the $+X$-direction. If the atom approaches on the left side, so that the reaction occurs for angles $0 \le \chi < \pi/2$, then the collision enhances the rotation of the product molecule and the final angular momentum is

$$L_X^{(f)} = -\frac{1}{m_A+m_B}r_e^{(f)}(m_A p_2 + m_B p_3 \cos\chi). \quad \text{(A20)}$$

Here, the direction of rotation is reversed with respect to the target molecule, just as two interlinking gears rotate in opposite directions when transferring their rotational motion to one another. The direction of the translational momentum is given by

$$\rho = \arctan\frac{|p_2 - \frac{m_B}{m_A+2m_B}p_{3\perp}|}{\alpha p_{3\parallel}}. \quad \text{(A21)}$$

The angle ρ can be converted to the planar scattering angle φ, which defines the direction of the translational motion of the scattered atom with respect to the space fixed coordinate system. If $p_2 > \frac{m_B}{m_A+2m_B}p_{3\perp}$, the scattering angle is $\varphi = \chi - \rho$, and for $p_2 \le \frac{m_B}{m_A+2m_B}p_{3\perp}$, it is $\varphi = \chi + \rho$. If the atom approaches from the right side, i.e., at $\pi/2 \le \chi \le \pi$,

$$L_X^{(f)} = -\frac{1}{m_A+m_B}r_e^{(f)}(m_A p_2 - m_B p_3 \cos\chi). \quad \text{(A22)}$$

Here, the collision can decelerate or stop the rotational motion if $m_A p_2 \ge m_B p_3 \cos\chi$. In this case, the product molecule rotates in the opposite direction as the target molecule. If $m_A p_2 < m_B p_3 \cos\chi$, the sense of rotation is reversed, and the product molecule rotates in the same direction as the initial molecule. The scattering angle is given by

$$\rho = \arctan\frac{|p_2 + \frac{m_B}{m_A+2m_B}p_{3\perp}|}{\alpha p_{3\parallel}} \quad \text{(A23)}$$

and $\varphi = \chi - \rho$. For a molecule with negative initial angular momentum, the two pathways are reversed.

For a better comparison with the differential cross section for the quantum mechanical simulation of the scattering process, we convert the planar scattering angle to azimuthal and polar scattering angles. Planar scattering angles in the range of $-90° < \varphi < 90°$ correspond to azimuthal scattering angle of $\phi = 90°$ with the polar scattering angle ranging from $\theta = 0$ for $\varphi = 90°$ to $\theta = 180°$ for $\varphi = -90°$. Scattering to the left ($90° < \varphi < 270°$) corresponds to $\phi = 270°$, with $\theta = 180°$ corresponding to $\varphi = 270°$. Note that in the following, the

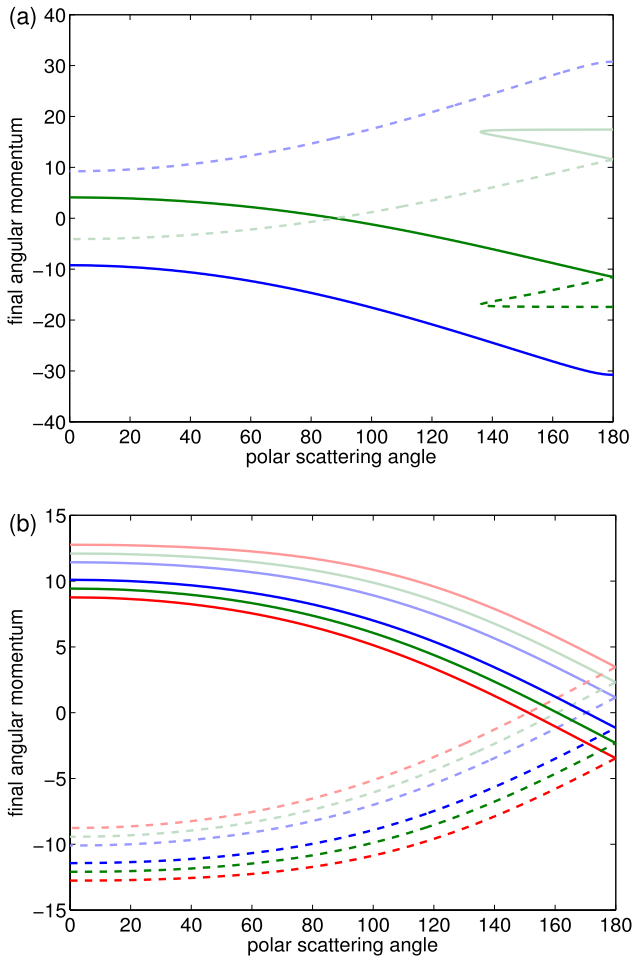

FIG. 16. Final angular momentum (in units of $\hbar$) as a function of the polar scattering angle θ for the reaction D + H_2 → HD + H. The solid (dashed) lines correspond to an azimuthal scattering angle of $\phi = 90°$ ($\phi = 270°$). In panel (a), the initial angular momentum is $L_X^{(i)} = \pm 10\hbar$ (green lines) and $L_X^{(i)} = \pm 30\hbar$ (blue lines). Here, $T_{rot} \ge T_{trans}$. In panel (b), $L_X^{(i)} = \pm 1\hbar$ (blue), $L_X^{(i)} = \pm 2\hbar$ (green), and $L_X^{(i)} = \pm 3\hbar$ (red), i.e., $T_{rot} \ll T_{trans}$. The bright and pale lines correspond to positive and negative initial angular momenta, respectively. The initial translational momentum is $p_{3y} \approx 32.3\hbar/r_e$ which corresponds to a collision energy of 1.0 eV. Here, the atomic masses are $m_B = m_H$ and $m_A = 2m_H$, with the hydrogen mass m_H. The equilibrium distance for initial and final molecules is $r_e^{(f)} \approx r_e = 0.74$ Å.

scattering angles define the direction in which the product HD molecule is scattered.

Figure 16 shows the final angular momentum as function of the polar scattering angle θ for the reaction $D+H_2 \rightarrow HD+H$ for target molecules with different rotational energies. If the initial rotational energy is much larger than the translational energy, as for $L_X^{(i)} = \pm 30\hbar$ which is shown as blue lines in Fig. 16(a), the product molecule always rotates in the opposite sense compared to the initial molecule, since the translational momentum is too small, compared to the rotational momentum, to reverse the direction of rotation. For a counter-clockwise rotating molecule (bright blue line), the atom is always scattered to the left, and the product molecule is scattered to the right. For clockwise rotating target molecules (pale blue line), the product molecule is scattered in the opposite direction. In this case, the sense of rotation can be immediately determined from the azimuthal scattering angle. Moreover, molecules with different sense of rotation can be separated from each other since they are scattered in opposite direction. If the initial rotational energy is comparable with the translational energy, as for $L_X^{(i)} = \pm 10\hbar$ (green lines in Fig. 16(a)), an interplay between rotational and translational momentum determines the scattering angle and the sense of rotation of the product molecule. Here, the translational momentum is large enough to stop and reverse the sense of rotation such that some product molecules have the same sense of rotation as the target molecules. Moreover, some of the counter-clockwise (clockwise) rotating molecules are scattered to the left (right). In a typical scattering experiment, only a few rotational states are excited initially, so the initial rotational energy is much smaller than the translational energy. This case is depicted in Fig. 16(b) for $L_X^{(i)} = \pm 1\hbar$ (blue), $\pm 2\hbar$ (green), and $\pm 3\hbar$ (red). Here, the product molecules are scattered in both in $\phi = 90°$ (solid lines) and in $\phi = 270°$ (dashed lines) direction. For counter-clockwise rotating target molecules, the product molecules with opposite sense of rotation are scattered predominantly to the left ($\phi = 270°$), while those which rotate in the same sense as the target molecules are scattered to the right $\phi = 90°$. As it is shown in Sec. III, this simple vector model shows good agreement with the quantum mechanical differential cross sections for the $D+H_2 \rightarrow HD+H$ reaction.

[1]J. Aldegunde, M. P. de Miranda, J. M. Haigh, B. K. Kendrick, V. Sáez-Rábanos, and F. J. Aoiz, J. Phys. Chem. A **109**, 6200 (2005).
[2]J. Aldegunde, J. M. Alvariño, B. K. Kendrick, V. Sáez-Rábanos, M. P. de Miranda, and F. J. Aoiz, Phys. Chem. Chem. Phys. **8**, 4881 (2006).
[3]J. Aldegunde, F. J. Aoiz, and M. P. de Miranda, Phys. Chem. Chem. Phys. **10**, 1139 (2008).
[4]T. Seideman and E. Hamilton, Adv. At., Mol., Opt. Phys. **52**, 289 (2005).
[5]M. Leibscher, I. Sh. Averbukh, and H. Rabitz, Phys. Rev. Lett. **90**, 213001 (2003); Phys. Rev. A **69**, 013402 (2004).
[6]S. Fleischer, Y. Khodorkovsky, Y. Prior, and I. Sh. Averbukh, New J. Phys. **11**, 10539 (2009).
[7]A. G. York, Opt. Express **17**, 23671 (2009).
[8]K. Kitano, H. Hasegawa, and Y. Ohshima, Phys. Rev. Lett. **103**, 223002 (2009).
[9]S. Fleischer, I. Sh. Averbukh, and Y. Prior, Phys. Rev. A **74**, 041403 (2006).
[10]S. Fleischer, I. Sh. Averbukh, and Y. Prior, Phys. Rev. Lett. **99**, 093002 (2007).
[11]I. Sh. Averbukh and E. Gershnabel, Phys. Rev. Lett. **104**, 153001 (2010); Phys. Rev. A **82**, 033401 (2010).
[12]Y. Khodorkovsky, J. R. Manson, and I. Sh. Averbukh, Phys. Rev. A **84**, 053420 (2011).
[13]T. Grohmann and M. Leibscher, J. Chem. Phys. **134**, 204316 (2011).
[14]S. Fleischer, Y. Khodorkovsky, E. Gershnabel, Y. Prior, and I. Sh. Averbukh, Isr. J. Chem. **52**, 414 (2012).
[15]C. J. Eyles and M. Leibscher, J. Chem. Phys. **139**, 104315 (2013).
[16]N. Mukherjee, W. Dong, and R. N. Zare, J. Chem. Phys. **140**, 074201 (2014).
[17]S. Zhdanovich, A. A. Milner, C. Bloomquist, J. Floß, I. Sh. Averbukh, J. W. Hepburn, and V. Milner, Phys. Rev. Lett. **107**, 243004 (2011).
[18]C. Bloomquist, S. Zhdanovich, A. A. Milner, and V. Milner, Phys. Rev. A **86**, 063413 (2012).
[19]J. Floß and I. Sh. Averbukh, Phys. Rev. A **86**, 063414 (2012).
[20]A. M. Arthurs and A. Dalgarno, Proc. R. Soc. London, Ser. A **256**, 540 (1960).
[21]Hibridon, a package of programs for the time-independent quantum treatment of inelastic collisions and photodissociation written by M. H. Alexander, D. Manolopoulos, H.-J. Werner, and B. Follmeg, with contributions by P. F. Vohralik, D. Lemoine, G. Corey, R. Gordon, B. Johnson, T. Orlikowski, A. Berning, A. D. Esposti, C. Rist, P. Dagdigian, B. Pouilly, G. van der Sanden, M. Yang, F. de Weerd, S. Gregurick, and J. Kłos.
[22]M. H. Alexander and D. E. Manolopoulos, J. Chem. Phys. **86**, 2044 (1987).
[23]D. Skouteris, J. F. Castillo, and D. E. Manolopoulos, Comput. Phys. Commun. **133**, 128 (2000).
[24]K. Blum, *Density Matrix Theory and Applications* (Plenum, New York, 1996).
[25]C. J. Eyles, M. Brouard, C.-H. Yang, J. Kłos, F. J. Aoiz, A. Gijsbertsen, A. E. Wiskerke, and S. Stolte, Nat. Chem. **3**, 597 (2011).
[26]J. Jankunas, R. N. Zare, F. Bouakline, S. C. Althorpe, D. Herráez-Aguilar, and F. J. Aoiz, Science **336**, 1687 (2012).
[27]J. Aldegunde, P. G. Jambrina, V. Sáez-Rábanos, M. P. de Miranda, and F. J. Aoiz, Phys. Chem. Chem. Phys. **12**, 13626 (2010).
[28]J. Aldegunde, P. G. Jambrina, M. P. de Miranda, V. Sáez-Rábanos, and F. J. Aoiz, Phys. Chem. Chem. Phys. **13**, 8345 (2011).
[29]F. Wang, J.-S. Lin, and K. Liu, Science **331**, 900 (2011).
[30]F. Wang, J.-S. Lin, and K. Liu, J. Chem. Phys. **140**, 084202 (2014).
[31]J. I. Cline, K. T. Lorenz, E. A. Wade, J. W. Barr, and D. W. Chandler, J. Chem. Phys. **115**, 6277 (2001).
[32]K. T. Lorenz, D. W. Chandler, J. W. Barr, W. Chen, G. L. Barnes, and J. I. Cline, Science **293**, 2063 (2001).
[33]R. N. Zare, *Angular Momentum* (Plenum, New York, 1988).
[34]S. Siegbahn and B. Liu, J. Chem. Phys. **68**, 2457 (1978).
[35]D. G. Truhlar and C. J. Horowitz, J. Chem. Phys. **68**, 2466 (1978).
[36]D. G. Truhlar and C. J. Horowitz, J. Chem. Phys. **71**, 1514 (1979).
[37]K. Stark and H.-J. Werner, J. Chem. Phys. **104**, 6515 (1996).
[38]F. Fernandez-Alonso, B. D. Bean, and R. N. Zare, J. Chem. Phys. **111**, 1035 (1999).
[39]M. P. de Miranda, F. J. Aoiz, V. Sáez-Rábanos, and M. Brouard, J. Chem. Phys. **121**, 9830 (2005).
[40]M. Hankel, S. C. Smith, R. J. Allan, S. K. Gray, and G. G. Balint-Kurti, J. Chem. Phys. **125**, 164303 (2006).
[41]L. Y. Rusin, M. B. Sevryuk, and J. P. Toennies, J. Chem. Phys. **122**, 134314 (2005).
[42]L. Y. Rusin, M. B. Sevryuk, and J. P. Toennies, "The HF(v′=3) forward scattering peak of the F + H_2 reaction revisited," e-print arXiv:1009.1578 [physics.chem-ph] (2010).
[43]V. Aquilanti, S. Cavalli, D. D. Fazio, A. Simoni, and T. V. Tscherbul, J. Chem. Phys. **123**, 054314 (2005).
[44]D. Sokolovshi, D. D. Fazio, S. Cavalli, and V. Aquilanti, Phys. Chem. Chem. Phys. **9**, 5664 (2007).